ADVANCED FUNCTIONAL MATERIALS

www.afm-journal.de

Single Component Organic Solar Cells Based on Oligothiophene-Fullerene Conjugate

Thanh Luan Nguyen, Tack Ho Lee, Bhoj Gautam, Song Yi Park, Kenan Gundogdu, Jin Young Kim,* and Han Young Woo**

A new donor (D)–acceptor (A) conjugate, benzodithiophene-rhodanine–[6,6]-phenyl-C_{61} butyric acid methyl ester (BDTRh–PCBM) comprising three covalently linked blocks, one of p-type oligothiophene containing BDTRh moieties and two of n-type PCBM, is designed and synthesized. A single component organic solar cell (SCOSC) fabricated from BDTRh–PCBM exhibits the power conversion efficiency (PCE) of 2.44% and maximum external quantum efficiency of 46%, which are the highest among the reported efficiencies so far. The SCOSC device shows efficient charge transfer (CT, ≈300 fs) and smaller CT energy loss, resulting in the higher open-circuit voltage of 0.97 V, compared to the binary blend (BDTRh:PCBM). Because of the integration of the donor and acceptor in a single molecule, BDTRh-PCBM has a specific D–A arrangement with less energetic disorder and reorganization energy than blend systems. In addition, the SCOSC device shows excellent device and morphological stabilities, showing no degradation of PCE at 80 °C for 100 h. The SCOSC approach may suggest a great way to suppress the large phase segregation of donor and acceptor domains with better morphological stability compared to the blend device.

1. Introduction

Organic solar cells (OSCs) are promising candidates for flexible and portable thin film photovoltaic (PV) cells due to their solution processabilty, light-weight, and mechanical flexibility.[1–4] Recently, bulk heterojunction (BHJ) OSCs comprising blended electron donor and acceptor (D and A) (such as n-type fullerene and nonfullerene derivatives) materials have demonstrated great advancements, showing 10–12% power conversion efficiency (PCE).[5–9] Outstanding PCEs have been achieved through extensive studies on photovoltaic material design, syntheses, and device fabrication, i.e., through studies on device architectures, morphology control, and interfacial engineering.[5–14] Ternary (or multiple) blend systems and tandem (or multijunction) device structures have also been investigated as a strategy to realize high performance OSCs. To further improve the PCE, the complexity in device architecture and the number of components in the device increases.[4,7,14,15]

BHJ thin film devices provide large interfaces between two components by forming nanosized donor–acceptor domains with bicontinuous interpenetrating networks, resulting in efficient charge separation and transport. The BHJ morphology is strongly dependent upon fabrication conditions and methods such as blend ratio, solvent, processing additive, casting methods (spin-coating, bar coating, doctor blade casting, etc.), and postprocessing (i.e., thermal and solvent vapor annealing).[5–17] Even if the ideal BHJ film morphology is achieved by optimizing the fabrication conditions, the morphology can easily change during device operation, because the kinetically frozen state gradually changes into the thermodynamically stable one. For example, fullerene derivatives tend to aggregate easily, resulting in the unfavorably large phase separation. The fine-control of phase separation in BHJ films is very difficult (not possible practically) and morphological imperfections induce drastic decrease in the device performance and stability.

As another interesting strategy, after Imahori's report on carotenoid-linked C60 in 1995,[18] single molecular donor–acceptor conjugates or all-in-one molecules where the donor and acceptor moieties are integrated by a covalent linkage in a single molecule have been reported for its potential as an alternative photovoltaic material.[19–34] Moreover, single component organic solar cells (SCOSCs) ensure very efficient (or fast) charge separation, because the exciton generation and dissociation may occur in the same molecule. Furthermore, simplified device fabrication without complicated processing steps can be expected with a suppression of the large phase

Dr. T. L. Nguyen, Prof. H. Y. Woo
Department of Chemistry
Korea University
Seoul 136-713, Republic of Korea
E-mail: hywoo@korea.ac.kr

T. H. Lee, S. Y. Park, Prof. J. Y. Kim
Department of Energy Engineering
Ulsan National Institute of Science and Technology (UNIST)
Ulsan 44919, Republic of Korea
E-mail: jykim@unist.ac.kr

Dr. B. Gautam, Prof. K. Gundogdu
Department of Physics
North Carolina State University
Raleigh, NC 27695, USA
E-mail: kenan_gundogdu@ncsu.edu

The ORCID identification number(s) for the author(s) of this article can be found under https://doi.org/10.1002/adfm.201702474.

DOI: 10.1002/adfm.201702474

segregation of donor and acceptor domains.[25] The SCOSC system does not rely on the donor–acceptor blend ratio, suggesting that a proper molecular design can lead to a stable phase separation for OSCs.[25] Nierengarten et al. reported the fulleropyrrolidine bearing oligophenylenevinylene, which can be considered as the first example of the all-in-one molecule designed for photovoltaic conversion.[26] Then, conjugated polymers (or oligomers) tethered with C60 derivatives,[25,29–32] non-fullerene based donor–acceptor conjugates,[25,30–32] nonconjugated and conjugated block copolymers have been also reported for SCOSC devices.[25,30–33] For example, Guo et al. successfully demonstrated the SCOSC using poly(3-hexylthiophene)–block–poly((9,9-dioctylfluorene)-2,7-diyl-*alt*-(4,7-bis(thiophen-5-yl)-2,1,3-benzothiadiazole)-2′,2″-diyl) (P3HT-*b*-PFTBT) as a single component active material with 3.1% of PCE.[34] In addition, several interesting approaches have been tried to prepare the all-in-one photovoltaic materials including dyads or triads based on azothiophene-fullerene, cyanine-fullerene, oligo(phenylene ethynylene)-fullerene, diketopyrrolopyrrole (DPP) containing oligothiophene-fullerene and dithienosilole-benzothiadiazole conjugated donor and two fullerene acceptors.[21,27,28] Hashimoto and co-workers reported 1.28–1.92% PCE based on the oligo(*p*-phenylene vinylene)-fullerene dyad with a highly crystalline donor moiety to increase the fill factor (FF). They claimed that covalent attachment of donor and acceptor in the dyad prevents large phase separation, resulting in good morphology and device stability compared to BHJ blend devices.[27] Singh and co-workers also reported a dyad of diathiafulvalene—functionalized DPP and fullerene for SCOSCs with 2.2% PCE, demonstrating broad light absorption tailing up to 1000 nm, and improved charge transporting property.[21] However, the PCE and external quantum efficiencies (EQEs) of SCOSC are still far behind those of blend devices.

SCOSCs have attracted less attention in the organic photovoltaic (OPV) community compared to multicomponents OPVs, because the design and development of ideal all-in-one photovoltaic molecules still represent a challenge. The molecular structure should be designed carefully to obtain the efficient charge generation and transport by forming bicontinuous crystalline domains of donors and acceptors. Detailed investigations of the charge dynamics, i.e., exciton generation, separation, and charge recombination are necessary in order to understand the charge dynamics in SCOSCs by comparing those in binary blend systems. The systematic studies of the molecular structure, morphology, charge dynamics, and resulting device properties are necessary to further optimize the SCOSCs.

2. Results and Discussion

2.1. Design, Synthesis and Characterization

In this study, we designed and synthesized a new all-in-one photovoltaic material and obtained the SCOSC with a PCE of 2.44% and a maximum EQE of 46%, which are among the highest efficiencies reported so far. Recently, Yang and co-workers reported the synthesis and electronic properties of a highly efficient 2D conjugated p-type small molecule named (5E,5′E)-5,5′-(5″,5‴″-(4,8-bis(5-(2-ethylhexyl)thiophen-2-yl)benzo[1,2-b:4,5-b′]dithiophene-2,6-diyl)-bis(3,3″-dioctyl-[2,2′:5′,2″-terthiophene]-5″,5-diyl)-bis(methanylylidene)-bis(3-octyl-2-thioxothiazolidin-4-one)) (SMPV1). Blended with [6,6]-phenyl-C_{71} butyric acid methyl ester ($PC_{71}BM$), SMPV1 showed a PCE of 8.02% for single junction OSCs and 10.1% for double junction homotandem OSCs.[35] Therefore, in this work, the same p-type structure was selected for designing an all-in-one molecule. In order to integrate p-type and n-type blocks, p-type block was functionalized with terminal hydroxyl groups. Detailed synthesis procedures are provided in **Scheme 1** and supporting information. Briefly, compounds 1 and 2 were prepared according to the reported procedure[36–38] and then coupled together to form the p-type block (benzodithiophene-rhodanine, BDTRh) via the Knoevenagel condensation.[38] BDTRh–[6,6]-phenyl-C_{61} butyric acid methyl ester (PCBM) was synthesized in 42% yield by connecting BDTRh with two PCBM wings via an esterification reaction.[27] The molecular structure of BDTRh–PCBM was confirmed by nuclear magnetic resonance (NMR) spectroscopy, high resolution mass spectrometry, and size exclusion chromatography (Figure S1, Supporting Information). The details are described in the Supporting information.

Figure 1b shows the normalized UV–vis absorption spectra of BDTRh and BDTRh–PCBM in chloroform and in film. Both compounds exhibit almost identical light absorption over a wide wavelength range of 300–600 nm (with maximum absorption at λ_{abs} = 505 nm) in solution and 300–700 nm (with maximum absorption at λ_{abs} = 577 nm for BDTRh and 557 nm for BDTRh–PCBM) in film. The broader and redshifted absorption in film (for both structures) indicates facile intermolecular aggregation in solid state. The clear shoulder peak at 650 nm for BDTRh suggests a stronger π–π stacking between neighboring molecules in BDTRh compared to the conjugate, BDTRh–PCBM. The bulky PCBM molecules at termini may hinder the tight intermolecular packing of the core BDTRh moieties in film for the all-in-one system. BDTRh–PCBM has a deeper highest occupied molecular orbital (–5.32 eV) energy level compared to that (–5.15 eV) of BDTRh, while both lowest unoccupied molecular orbital energy levels are at –3.55 eV (Figure 1c). As a result, the bandgap of BDTRh–PCBM is slightly larger than that of BDTRh (Table S1, Supporting Information). Cyclic voltammograms of BDTRh and BDTRh–PCBM are shown in Figure S2a in the Supporting Information. Thermal stability of BDTRh–PCBM and BDTRh was analyzed by thermogravimetric analysis (Figure S2b, Supporting Information) and differential scanning calorimetry (Figure S2c, Supporting Information). BDTRh–PCBM and BDTRh showed the decomposition onset temperatures with 5% weight loss at 388 and 405 °C, respectively. A melting temperature at 173 °C and a recrystallization point at 152 °C were measured for BDTRh. However, no temperature transition points were observed in the range of 25–250 °C for BDTRh–PCBM. The reduced crystallinity of BDTRh–PCBM is possibly due to the bulky terminal PCBM units, resulting in hindering the packing of the BDTRh core.

Photoluminescence (PL) spectra of BDTRh, BDTRh:PCBM blend, and BDTRh-PCBM were measured in dilute chloroform solution ($\approx 3 \times 10^{-6}$ M). As shown in Figure S3 in the Supporting Information, the diluted BDTRh:PCBM blend solution shows negligible PL quenching compared to that of BDTRh.

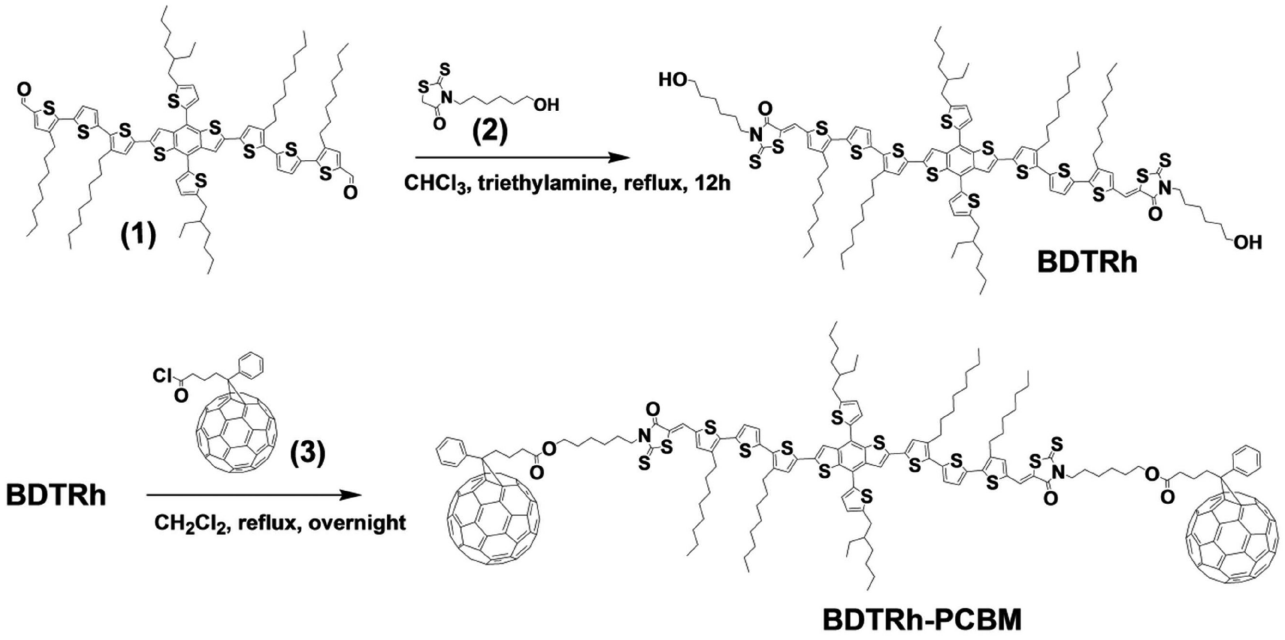

Scheme 1. Synthesis of BDTRh and BDTRh-PCBM.

However, the chemically bonded BDTRh-PCBM shows clearly the decreased PL emission due to facile intramolecular charge transfer from BDTRh to PCBM in the same molecule. The PL data confirm the efficient intramolecular charge separation in the single molecular BDTRh-PCBM compared to the blend system.

2.2. Photovoltaic Characterization

The photovoltaic characteristics were investigated by fabricating conventional OSC devices based on indium tin oxide (ITO)/poly(3,4-ethylenedioxythiophene): polystyrene sulfonic acid (PEDOT:PSS)/photoactive layer/ZnO/Al with a BDTRh–PCBM component as a photoactive layer for SCOSC. For comparison, a binary blend device based on BDTRh:PCBM was also prepared (Figure S4 and Table S2, Supporting Information). A blend ratio of 1:2 for BDTRh:PCBM (by mole) was chosen to compare the device properties. The current density–voltage (J–V) characteristics of BDTRh–PCBM device are displayed in **Figure 2**a. In order to optimize the fabrication of SCOSC, processing additives and postprocessing methods (e.g., solvent vapor annealing and thermal annealing) were tested. In addition, a ZnO layer was incorporated as an electron-transporting layer between the photoactive layer and Al cathode,[39,40] increasing both the short-circuit current density (J_{SC}) and FF of SCOSCs (Figure S5 and Table S3, Supporting Information). However, the processing additive, thermal, and solvent vapor annealing were not effective to modulate the film morphology and electrical properties of SCOSCs, because both donor and acceptor moieties are chemically connected and phase separation modulation may be difficult compared to BHJ blends. The SCOSC fabrication was optimized without any postprocessing (Table S4, Supporting Information). The best PCE of SCOSC was determined to be 2.44% with J_{SC} of 7.02 mA cm^{-2}, open-circuit voltage (V_{OC}) of 0.97 V, and FF of 0.36. For comparison, the binary blend device was prepared under the same conditions, showing photovoltaic characteristics with PCE = 2.31% (J_{SC} of 5.2 mA cm^{-2}, V_{OC} of 0.88 V, and FF of 0.52). The measured PCE (2.44%) is among the highest PCEs for C60-π-conjugated molecular SCOSCs reported so far.[19–21,41,42] The EQE spectrum of BDTRh–PCBM follows the UV–vis absorption of the thin film with the onset wavelength of ≈697 nm (Figure 2b) and the maximum EQE of SCOSCs was measured to be 46% at 420 nm. Although the BDTRh–PCBM SCOSC successfully demonstrated a great potential with the PCEs over 2%, its photovoltaic performance is still far behind that of well performing BHJ blend devices. The charge dynamics and morphological features are expected to be different from those in the typical blend devices, which should be studied thoroughly. We investigated the light intensity dependent photovoltaic characteristics and charge mobilities in both parallel and vertical directions.

Light intensity dependencies of J_{SC} and V_{OC} were measured to investigate charge carrier recombination in the device (Figure 2c,d). The J_{SC} versus light intensity curve was fitted according to a power-law equation, $J_{SC} \propto I^{\alpha}$ (where I is the light intensity and α indicates a slope of a logarithmic plot of J_{SC} vs light intensity). The slope in the log–log plot of J_{SC} versus light intensity was determined to be 0.94 for the BDTRh–PCBM SCOSC. The semilogarithmic plot of V_{OC} versus light intensity shows that the slope of BDTRh–PCBM is 1.18 kT/q, where k is the Boltzmann constant, T is the absolute temperature, and q is the electron charge. Both experiments suggest that the SCOSC device suffers from significant bimolecular and trap assisted charge recombination as seen in inferior J_{SC} and FF.[43–45] The J–V characteristics in the dark and photocurrent (J_{ph}) versus effective voltage (V_{eff}) measurements were tested to investigate charge generation and extraction by comparing those of

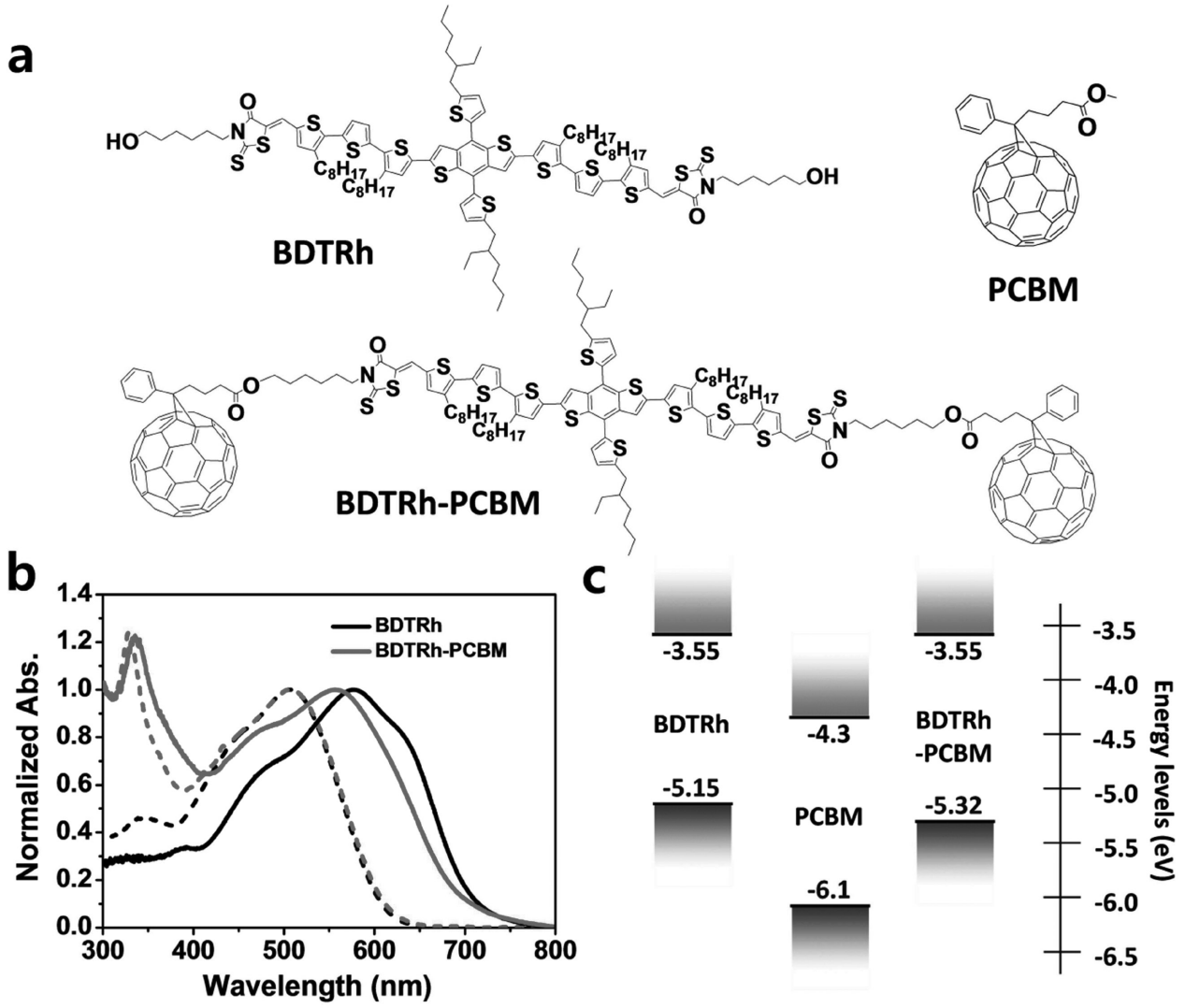

Figure 1. a) Molecular structures of photoactive materials, b) normalized UV–vis absorption spectra in chloroform (dashed) and in film (solid), and c) their energy levels.

typical blend devices (Figure S6, Supporting Information). The J_{ph} versus V_{eff} plot shows no saturation in the photocurrent, pointing to difficulties in charge collection, and extraction to electrodes in the SCOSC device.[44,46] Two bulky PCBMs connected to the core are expected to hinder the facile intermolecular packing of the core BDTRh moieties, blocking appropriate morphology modulation. In the chemically coupled D–A conjugates, the photoinduced electron transfer must be efficient, but the electron–hole recombination is also expected to be efficient if a bicontinuous and interconnected D–A network is not formed.

The morphologies of both BDTRh:PCBM and BDTRh–PCBM films were investigated by atomic force microscopy (AFM) and grazing incidence wide angle X-ray scattering (GIWAXS). Topological images and corresponding phase images are shown in Figure S7 in the Supporting Information. The BDTRh:PCBM blend film exhibited large phase separation with high root-mean-square (RMS) roughness value of 16.7 nm, while the single-molecule BDTRh–PCBM film had a homogeneous and flat surface (RMS roughness of 0.405 nm). Compared to the blend film, the BDTRh–PCBM film with covalently connected donor and acceptors shows less tendency to self-aggregate. GIWAXS measurements were carried out to investigate the intermolecular packing and orientations in SCOSC by comparison with those of binary BHJ device. The 2D GIWAXS images of the pristine BDTRh, BDTRh:PCBM blend, and single-molecular BDTRh–PCBM films are displayed in **Figure 3**. Packing parameters derived from GIWAXS measurements are summarized in Table S5 in the Supporting Information. The pristine BDTRh film has a strong (100) out-of-plane interlamellar scattering peak and (010) π–π stacking peaks in both in-plane and out-of-plane directions. By blending with PCBM, a new hump-shaped scattering peak appears due to the aggregated PCBMs. Similar scattering features were observed as for BDTRh, where donor and acceptor molecules form their own domains with large phase separation, as shown in AFM measurements. Additionally, the single-molecular BDTRh–PCBM film has a weak and broad (100) interlamellar packing

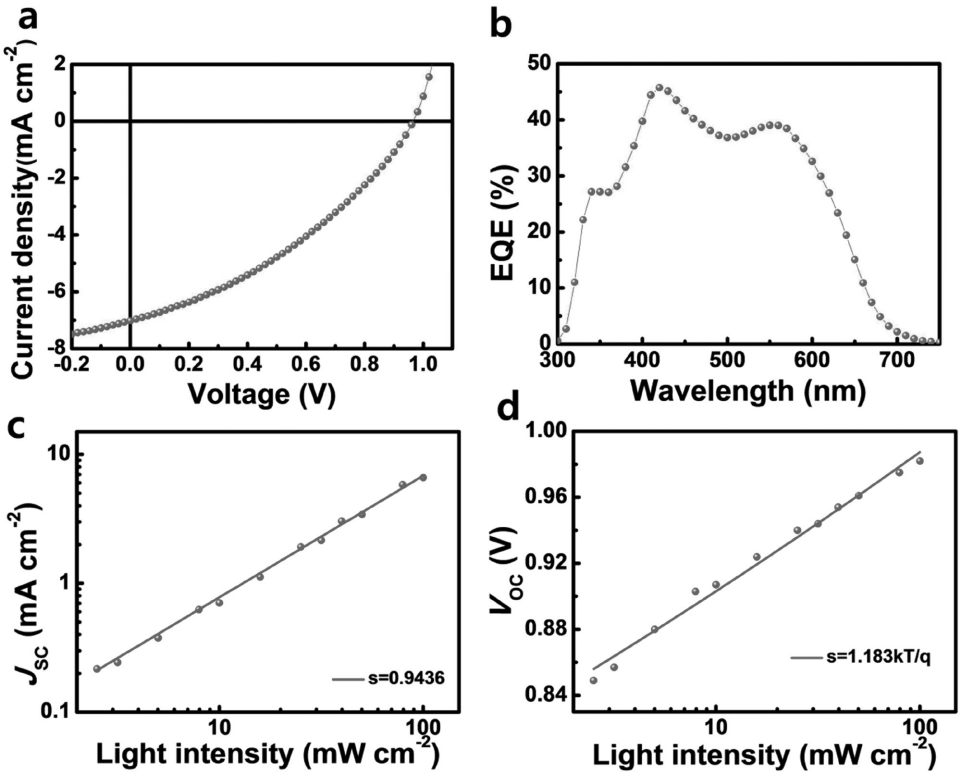

Figure 2. a) *J–V* characteristics, b) EQE spectra, light intensity dependence of c) J_{SC} and d) V_{OC} of BDTRh-PCBM SCOSCs.

peak from the BDTRh core and no (010) peaks, pointing to a significantly hindered intermolecular π–π packing of the BDTRh core in the dumbbell shaped BDTRh–PCBM.

We also tested the morphological and PCE stability of the two types of cells. The blend and SCOSC devices were prepared and their photovoltaic property decay was monitored at 80 °C for 100 h inside a glove box. As shown in **Figure 4**, the BDTRh:PCBM blend device shows a quick decay in PCE to ≈80% of the initial value in 10 min. The corresponding AFM surface morphology shows large phase segregation, suggesting poor morphological stability via facile aggregation of PCBMs (Figure S8, Supporting Information). Contrary to the

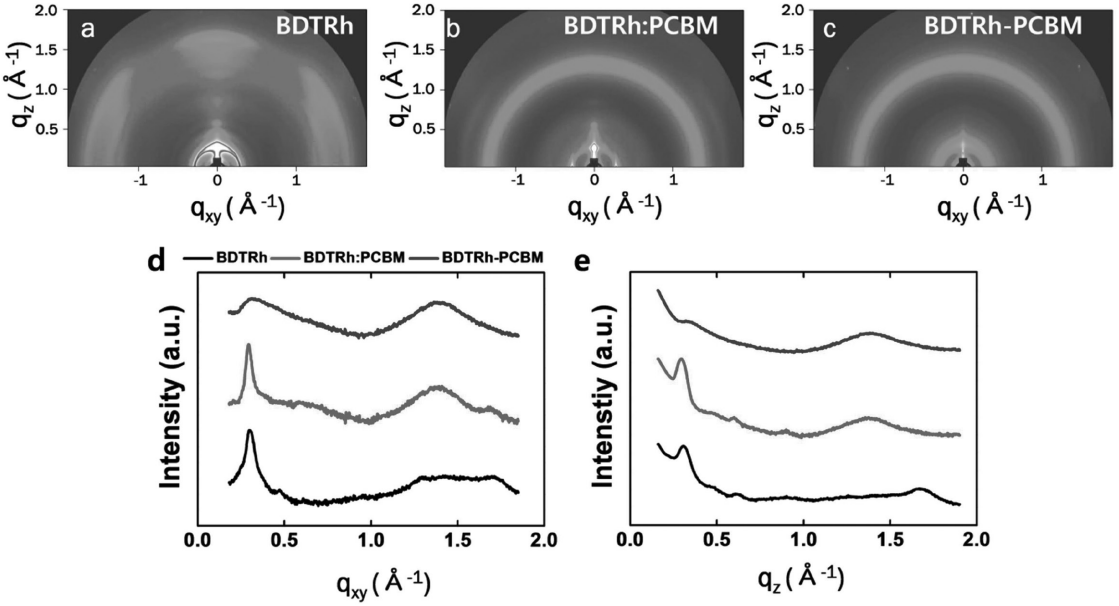

Figure 3. 2D GIWAXS images of a) BDTRh, b) BDTRh:PCBM, and c) BDTRh-PCBM films. Corresponding line-cuts in d) in-plane and e) out-of-plane directions. Films are represented in the top data sets.

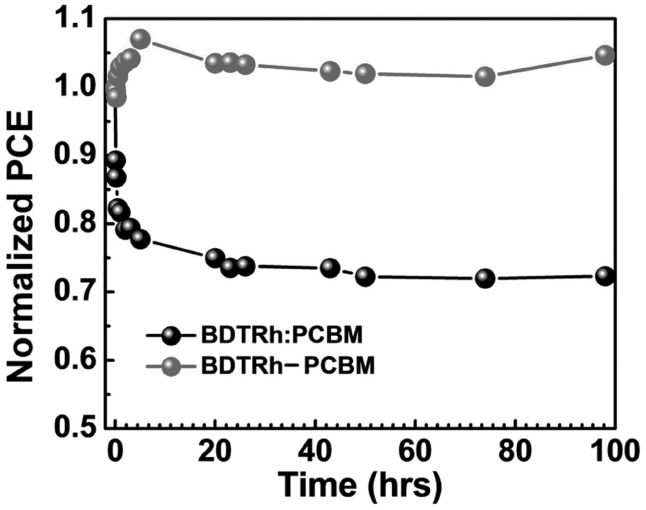

Figure 4. Device stability of BDTRh:PCBM and BDTRh-PCBM photovoltaic cells at an annealing temperature of 80 °C for 100 h.

blend system, the SCOSC device shows excellent device and morphological stabilities, showing no degradation of PCE at 80 °C for 100 h. There was no clear change in the surface morphology of the single molecular BDTRh-PCBM device, either. It clearly confirms that all-in-one photovoltaic materials suggest a great way to improve the morphological stability with a suppression of the large phase segregation of donor and acceptor domains.

To examine charge carrier transport characteristics of the BDTRh and BDTRh–PCBM films, organic field effect transistors were fabricated (Figure S9 and Table S6, Supporting Information). The detailed device fabrication methods are described in the Experimental Section. The typical p-type characteristics were measured in the transfer characteristics of BDTRh (core, Figure S9a, Supporting Information), but the all-in-one BDTRh–PCBM shows ambipolar transfer characteristics (Figure S9b, Supporting Information) due to a presence of both p- and n-type moieties in the single molecule. The extracted hole mobility (μ_h) of BDTRh was 1.15×10^{-4} cm^2 V^{-1} s^{-1}. However, substantially lower (by ≈2 orders) hole and electron mobility (μ_e) values were measured to be 1.03×10^{-6} and 8.96×10^{-6} cm^2 V^{-1} s^{-1} for BDTRh–PCBM, probably due to imperfections of film morphology caused by incomplete packing or misalignment in core parts of all-in-one molecules in the film. The space charge limited current was also measured to investigate charge carrier transport properties in a vertical direction (Figure S10, Supporting Information). Hole-only (ITO/PEDOT:PSS/photoactive layer/Au) and electron-only (fluorine-doped tin oxide (FTO)/photoactive layer/Al) devices were fabricated under the same fabrication conditions for the optimized SCOSC device.[10,47] Both hole and electron mobilities of SCOSCs were determined to be ≈10^{-6} cm^2 V^{-1} s^{-1}. The vertical charge mobility values of SCOSCs are ≈2 or 3 orders of magnitude lower than those of well performing BHJ devices. The inferior charge transport properties of BDTRh–PCBM are expected to originate from the amorphous film morphology confirmed by AFM and GIWAXS.

2.3. Charge Dynamics by Transient Absorption Spectroscopy

Steady-state PL was recorded on neat BDTRh, BDTRh:PCBM blend, and BDTRh–PCBM to study the exciton separation. The excitation energy was 2.17 eV in order to predominantly excite the BDTRh component in the blend and all-in-one system (Figure S11a, Supporting Information). The PL spectra of neat BDTRh, BDTRh:PCBM blend, and BDTRh–PCBM are shown in Figure S11b in the Supporting Information. By comparison with the neat film, the PL emission from BDTRh:PCBM blend film was strongly quenched (94.8%). In addition, the PL from all-in-one system was also quenched completely (96.4%). Both observations indicate that there is efficient electron transfer from the BDTRh moiety to PCBM in the heterojunction as well as in the BDTRh–PCBM molecule (also supported by transient absorption data discussed later).

In order to monitor the exciton and charge generation and recombination dynamics, we performed femtosecond transient absorption spectroscopy (TAS) for the BDTRh, BDTRh:PCBM blend, and BDTRh–PCBM. In these experiments, the excitation pulse (pump) is tuned to 2.17 eV in order to selectively excite the BDTRh component and the resulting dynamics is monitored by measuring the differential transmission of broad band probe pulses in the near IR region of the spectra at different time delays after the excitation. Figure S12a in the Supporting Information displays the results for the TAS of neat BDTRh film at different time delays. In the transient absorption spectra, a broad negative band centered at ≈1 eV and a positive band centered at ≈1.5 eV are observed. These bands (peaks) correspond to the excited state absorption of singlet excitons in BDTRh and to the stimulated emission, respectively. The dynamics of the negative band is shown in Figure S12b in the Supporting Information. Singlet excitons in BDTRh decay with the lifetime of 20 ps (1/e time). **Figure 5**a,b displays the TAS results at different time delays for BDTRh:PCBM blend and BDTRh–PCBM. We observed a strong polaron band centered at ≈1.4 eV in both samples in addition to exciton band at ≈1.03 eV. The assignments of the exciton and polaron photoinduced absorption spectral features are consistent with earlier results of TAS in polymer blends.[48–50] Figure 5c,d shows the time evolution of features at ≈1.03 and ≈1.4 eV for BDTRh:PCBM blend and BDTRh–PCBM. The singlet excitons undergo ultrafast charge transfer in both samples as indicated by the rapid decay of singlet exciton band at ≈1.03 eV. The decay time (2 ps) in BDTRh:PCBM blend is reduced by one order of magnitude compared to that in neat BDTRh (20 ps), indicating efficient photoinduced charge transfer. We also monitored the dynamics of the polaron peak at ≈1.4 eV. The polaron lifetime in this blend is 350 ps (1/e time). In BDTRh–PCBM, the electron transfer time is only 300 fs and the polaron lifetime (3.5 ns) is one order of magnitude longer compared to that in BDTRh:PCBM.

Interestingly, we observed an increase in the transient signal of the 1.03 eV (exciton peak) peak at longer delays for both BDTRh:PCBM blend and BDTRh–PCBM, indicating reformation of excitons after charge generation. This rise is previously observed and attributed to triplet generation due to back recombination of separated charges. It is mostly due to bimolecular recombination of charges. In order to test this possibility of bimolecular recombination, we performed intensity dependent

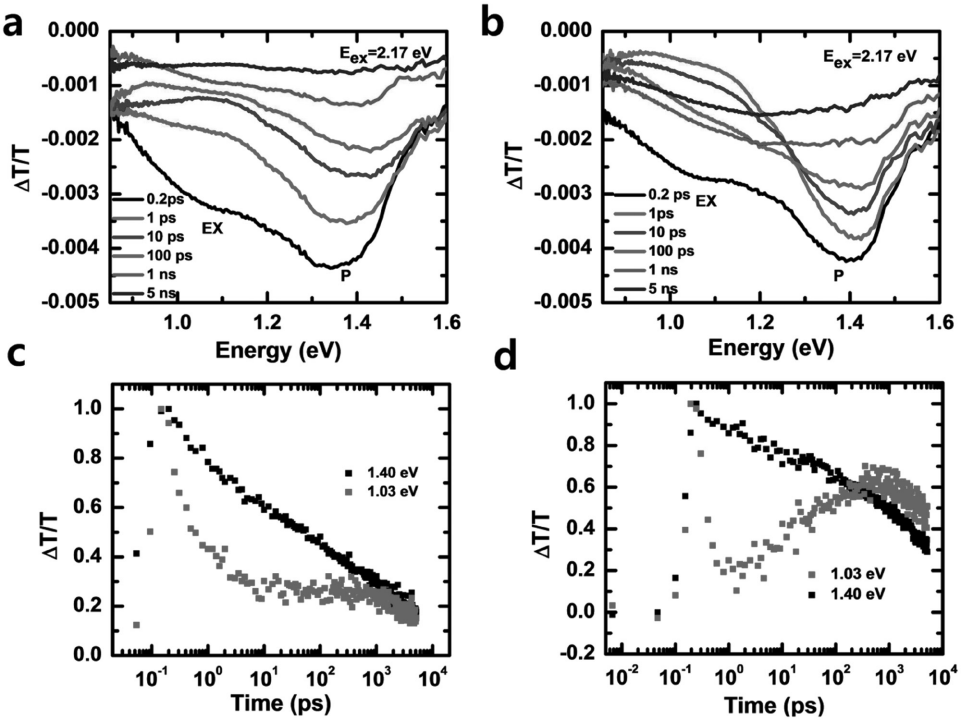

Figure 5. Transient absorption spectra of a) BDTRh:PCBM b) BDTRh-PCBM. Exciton and polaron dynamics of c) BDTRh:PCBM d) BDTRh-PCBM. EX and P in (a) and (b) refer to exciton and polaron, respectively.

TAS illustrated in Figure S13 in the Supporting Information. In the first few picoseconds, the decay dynamics of 1.03 eV peak is excitation intensity independent, which suggests no significant exciton–exciton annihilation in the material. However the rise of the peak shows significant excitation intensity dependence at longer delays (Figure S13a,b, Supporting Information), which is consistent with triplet exciton generation through the bimolecular recombination of electrons and holes. Bimolecular recombination is further supported by the strong intensity dependence of the polaron peak decay (Figure S13c,d, Supporting Information). Nongeminate recombination of charges increases with increasing intensity since charges are not extracted in these measurements (0 V bias). The triplet formation is much stronger in BDTRh–PCBM compared to that in the BDTRh:PCBM blend, while the photoexcitation density is similar.

We investigated D/A intermolecular charge transfer (CT) state energies of the binary blend and SCOSC devices. It should be noted that the SCOSC has a higher V_{OC} compared to that of the blend device (Figure S4 and Table S2, Supporting Information). It is very important to understand the origin of energy loss in the BHJ blend and SCOSC for further optimization of SCOSCs. As shown in **Figure 6**a, the EQE spectra in the CT region are plotted and CT bands are fitted using the following equation

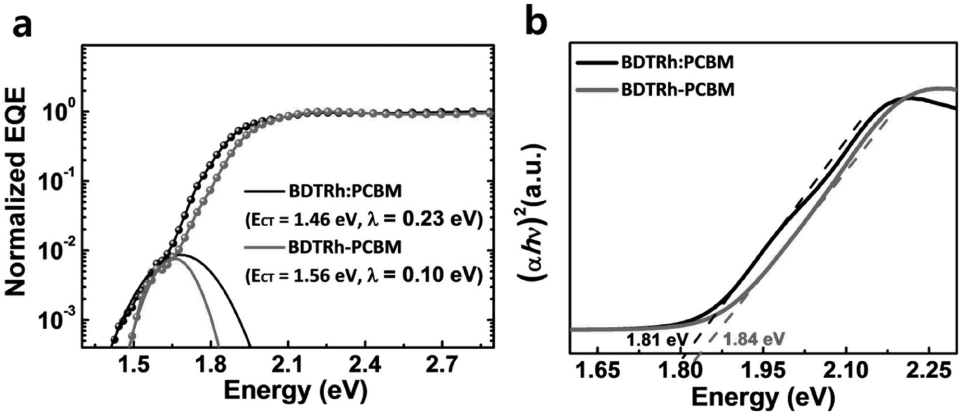

Figure 6. a) Comparison of EQE spectra in the CT region of BDTRh:PCBM and BDTRh-PCBM devices; the solid lines are fitting curves by Equation (1). b) Tauc plots of BDTRh:PCBM and BDTRh-PCBM films.

$$\mathrm{EQE}(E) = \frac{f}{E\sqrt{4\pi\lambda kT}} \exp\left(\frac{-(E_{CT}+\lambda-E)^2}{4\lambda kT}\right) \quad (1)$$

Here, E is the photon energy, k is the Boltzmann constant, and T is the absolute temperature. In this equation, f, E_{CT}, and λ are fitting parameters. Prefactor f is proportional to the number of states, E_{CT} is the energy of the excited CT state, and λ is related to the width of the CT absorbance band that is related to the reorganization energy term (λ_0).[51–54]

We estimated the energy loss resulting from charge transfer by the difference between the energy of the excited photoactive components (E_g) and E_{CT}: (E_g–E_{CT}). The value of E_g corresponds to the optical bandgap of photoactive components. It was derived from Tauc plots ($h\nu$–$E_g = (\alpha h\nu)^2$ for direct allowed transition, $h\nu$ is the light energy, α is the absorption coefficient) of BDTRh:PCBM and BDTRh–PCBM films (Figure 6b). The E_{CT} values from fitting curves were determined to be 1.46 and 1.56 eV for the BDTRh:PCBM blend and single molecular BDTRh–PCBM, respectively. The empirical relationship between V_{OC} and E_{CT} ($V_{OC} \cong E_{CT}/q - 0.6$, q is unit charge) shows that the estimated E_{CT} values are consistent with the measured V_{OC}.[55] The E_g–E_{CT} value for the SCOSC device was calculated to be 0.28 eV (=1.84–1.56 eV), which is smaller than that for the BDTRh:PCBM blend device (0.35 eV). The improvement of V_{OC} in the SCOSC system is supported by decreasing the energy losses resulting from the D/A interface charge transfer.

Another fitting parameter λ is related to the intermolecular charge transfer state arrangement and energetic disorder.[51,52] The λ value is reduced by forming a specific molecular arrangement that decreases energetic disorder and facilitates charge separation. The SCOSC has lower λ value (0.10 eV) compared to the bimolecular blend device (0.23 eV). This indicates that SCOSCs have more specific CT states and less energetic disorder compared to blend devices. In other words, the dumbbell shaped A–D–A structure of BDTRh–PCBM has a special D/A arrangement, which is considered to be advantageous for the energetic disorder reduction.

3. Conclusion

We successfully demonstrated a single molecular D–A conjugate based SCOSC with PCE of 2.44%. The photovoltaic characteristics of the SCOSC compared to the bimolecular blend system were investigated. Energy losses in CT processes in the SCOSC are substantially reduced, providing improved V_{OC}. By forming a specific molecular arrangement at the D/A interfaces, the intermolecular CT states arrangement and energetic disorder can be decreased in SCOSCs. In addition, we observed strong polaron band, ultrafast electron transfer, and strong triplet exciton formation in the SCOSC system. Our results suggest that the low charge mobility and recombination limit the photovoltaic performance despite the efficient charge generation on ultrafast time scale (≈300 fs) in SCOSC devices. To further improve the SCOSC device performance, the attention should be directed toward the optimization of film morphology by careful design of single molecular D–A conjugates. The D/A molar ratio and alkyl spacer between D and A blocks should be designed carefully by considering the crystalline ordering of D and A blocks to form an ideal bicontinuous interpenetrating D–A nanomorphology for efficient charge generation and transport. SCOSC technology may offer an important approach to improve the morphological and device stabilities by suppressing the large phase segregation of donor and acceptor domains, compared to the blend device. Despite all remaining challenges, the advent of this new type of devices paves a way for further development of OSCs.

Supporting Information

Supporting Information is available from the Wiley Online Library or from the author.

Acknowledgements

T.L.N. and T.H.L. contributed equally to this work. This work was supported by the National Research Foundation (NRF) of Korea (Nos. 2016M1A2A2940911, 2015M1A2A2057506, and 2012M3A6A7055540). TAS experiment carried out at North Carolina State University was supported by Office of Naval Research (ONR) Grant No. N000141310526 P00002. The 500 MHz NMR data were collected in the NMR Laboratory of center for Molecular Spectroscopy, Institute for Basic Science, in Korea University.

Conflict of Interest

The authors declare no conflict of interest.

Keywords

charge transfer, energy loss, organic photovoltaics, single component solar cells, transient absorption spectroscopy

Received: May 9, 2017
Revised: June 10, 2017
Published online: August 28, 2017

[1] C. J. Brabec, S. Gowrisanker, J. J. Halls, D. Laird, S. Jia, S. P. Williams, *Adv. Mater.* **2010**, *22*, 3839.
[2] a) A. J. Heeger, *Adv. Mater.* **2014**, *26*, 10; b) B. C. Thompson, J. M. Frechet, *Angew. Chem. Int. Ed.* **2008**, *47*, 58.
[3] B. Walker, C. Kim, T.-Q. Nguyen, *Chem. Mater.* **2011**, *23*, 470.
[4] J. Y. Kim, K. Lee, N. E. Coates, D. Moses, T.-Q. Nguyen, M. Dante, A. J. Heeger, *Science* **2007**, *317*, 222.
[5] V. Vohral, K. Kawashima, T. Kakara, T. Koganezawa, I. Osaka, K. Takimiya, H. Murata, *Nat. Photonics* **2015**, *9*, 403.
[6] W. Zhao, D. Qian, S. Zhang, S. Li, O. Inganäs, F. Gao, J. Hou, *Adv. Mater.* **2016**, *28*, 4734.
[7] S. Li, L. Ye, W. Zhao, S. Zhang, S. Mukherjee, H. Ade, J. Hou, *Adv. Mater.* **2016**, *28*, 9423.
[8] Y. Yang, Z.-G. Zhang, H. Bin, S. Chen, L. Gao, L. Xue, C. Yang, Y. Li, *J. Am. Chem. Soc.* **2016**, *138*, 15011.
[9] H. Kang, W. Lee, J. Oh, T. Kim, C. Lee, B. J. Kim, *Acc. Chem. Res.* **2016**, *49*, 2424.
[10] T. H. Lee, M. A. Uddin, C. Zhong, S.-J. Ko, B. Walker, T. Kim, Y. J. Yoon, S. Y. Park, A. J. Heeger, H. Y. Woo, J. Y. Kim, *Adv. Energy Mater.* **2016**, *6*, 1600637.

[11] Y. Liu, J. Zhao, Z. Li, C. Mu, W. Ma, H. Hu, K. Jiang, H. Lin, H. Ade, H. Yan, *Nat. Commun.* **2014**, *5*, 5293.
[12] H. Choi, S.-J. Ko, Y. Choi, P. Joo, T. Kim, B. R. Lee, J.-W. Jung, H. J. Choi, M. Cha, J.-R. Jeong, I.-W. Hwang, M. H. Song, B.-S. Kim, J. Y. Kim, *Nat. Photonics* **2013**, *7*, 732.
[13] S. Nho, G. Baek, S. Park, B. R. Lee, M. J. Cha, D. C. Lim, J. H. Seo, S.-H. Oh, M. H. Song, S. Cho, *Energy Environ. Sci.* **2016**, *9*, 240.
[14] B.-K. Yu, D. Vak, J. Jo, S.-I. Na, S.-S. Kim, Y.-S. Jung, D.-Y. Kim, *Macromol. Res.* **2015**, *7*, 696.
[15] S.-J. Ko, W. Lee, H. Choi, B. Walker, S. Yum, S. Kim, T. J. Shin, H. Y. Woo, J. Y. Kim, *Adv. Energy Mater.* **2015**, *5*, 1401687.
[16] Y.-H. Ha, J. E. Lee, M.-C. Hwang, Y. J. Kim, J.-H. Lee, C. E. Park, Y.-H. Kim, *Macromol. Res.* **2016**, *24*, 457.
[17] S. D. Collins, N. A. Ran, M. C. Heiber, T.-Q. Nguyen, *Adv. Energy Mater.* **2017**, *7*, 1602242.
[18] H. Imahori, S. Cardoso, T. Tatman, S. Lin, L. Noss, G. R. Seely, L. Sereno, J. C. de Silber, T. A. Moore, A. L. Moore, D. Gust, *Photochem. Photobiol.* **1995**, *62*, 1009.
[19] S. Izawa, K. Hashimoto, K. Tajima, *Phys. Chem. Chem. Phys.* **2012**, *14*, 16138.
[20] S. Izawa, K. Hashimoto, K. Tajima, *Chem. Commun.* **2011**, *47*, 6365.
[21] K. Narayanaswamy, A. Venkateswararao, P. Nagarjuna, S. Bishnoi, V. Gupta, S. Chand, S. P. Singh, *Angew. Chem. Int. Ed.* **2016**, *55*, 12334.
[22] M. Sommer, S. Hüttner, U. Steiner, M. Thelakkat, *Appl. Phys. Lett.* **2009**, *95*, 183308.
[23] S. Miyanishi, Y. Zhang, K. Tajima, K. Hashimoto, *Chem. Commun.* **2010**, *46*, 6723.
[24] L. Bu, X. Guo, B. Yu, Y. Qu, Z. Xie, D. Yan, Y. Geng, F. Wang, *J. Am. Chem. Soc.* **2009**, *131*, 13242.
[25] J. Roncali, *Adv. Energy Mater.* **2011**, *1*, 147.
[26] J.-F. Nierengarten, J.-F. Eckert, J.-F. Nicoud, L. Ouali, V. Krasnikov, G. Hadziioannou, *Chem. Commun.* **1999**, 617.
[27] S. Izawa, K. Hashimoto, K. Tajima, *Phys. Chem. Chem. Phys.* **2012**, *14*, 16138.
[28] J. Cao, X. Du, S. Chen, Z. Xiao, L. Ding, *Phys. Chem. Chem. Phys.* **2014**, *16*, 3512.
[29] Z. Tan, J. Hou, Y. He, E. Zhou, C. Yang, Y. Li, *Macromolecules* **2007**, *40*, 1868.
[30] J. L. Segura, N. Martín, D. M. Guldi, *Chem. Soc. Rev.* **2005**, *34*, 31.
[31] A. Cravino, *Polym. Int.* **2007**, *56*, 943.
[32] J. Roncali, *Chem. Soc. Rev.* **2005**, *34*, 483.
[33] S. Koyuncu, H. W. Wang, F. Liu, K. B. Toga, W. Gu, T. P. Russell, *J. Mater. Chem. A* **2014**, *2*, 2993.
[34] C. Guo, Y.-H. Lin, M. D. Witman, K. A. Smith, C. Wang, A. Hexemer, J. Strzalka, E. D. Gomez, R. Verduzco, *Nano Lett.* **2013**, *13*, 2957.
[35] Y. Liu, C.-C. Chen, Z. Hong, J. Gao, Y. Yang, H. Zhou, L. Dou, G. Li, Y. Yang, *Sci. Rep.* **2013**, *3*, 3356.
[36] A. Tang, C. Zhan, J. Yao, *Chem. Mater.* **2015**, *27*, 4719.
[37] C. Nitsche, V. N. Schreier, M. A. M. Behnam, A. Kumar, R. Bartenschlager, C. D. Klein, *J. Med. Chem.* **2013**, *56*, 8389.
[38] J. Zhou, Y. Zuo, X. Wan, G. Long, Q. Zhang, W. Ni, Y. Liu, Z. Li, G. He, C. Li, B. Kan, M. Li, Y. Chen, *J. Am. Chem. Soc.* **2013**, *135*, 8484.
[39] M. Moon, B. Walker, J. Lee, S. Y. Park, H. Ahn, T. Kim, T. H. Lee, J. Heo, J. H. Seo, T. J. Shin, J. Y. Kim, C. Yang, *Adv. Energy Mater.* **2015**, *5*, 1402044.
[40] A. K. Kyaw, D. H. Wang, D. Wynands, J. Zhang, T. Q. Nguyen, G. C. Bazan, A. J. Heeger, *Nano Lett.* **2013**, *13*, 3796.
[41] T. Nishizawa, H. K. Lim, K. Tajima, K. Hashimoto, *Chem. Commun.* **2009**, 2469.
[42] T. Nishizawa, K. Tajima, K. Hashimoto, *J. Mater. Chem.* **2007**, *17*, 2440.
[43] S. R. Cowan, A. Roy, A. J. Heeger, *Phys. Rev. B* **2010**, *82*, 245207.
[44] M. A. Uddin, T. H. Lee, S. Xu, S. Y. Park, T. Kim, S. Song, T. L. Nguyen, S.-J. Ko, S. Hwang, J. Y. Kim, H. Y. Woo, *Chem. Mater.* **2015**, *27*, 5997.
[45] L. J. A. Koster, V. D. Mihailetchi, R. Ramaker, P. W. M. Blom, *Appl. Phys. Lett.* **2005**, *86*, 123509.
[46] L. J. A. Koster, V. D. Mihailetchi, H. Xie, P. W. M. Blom, *Appl. Phys. Lett.* **2005**, *87*, 203502.
[47] T. L. Nguyen, H. Choi, S. J. Ko, M. A. Uddin, B. Walker, S. Yum, J. E. Jeong, M. H. Yun, T. J. Shin, S. Hwang, J. Y. Kim, H. Y. Woo, *Energy Environ. Sci.* **2014**, *7*, 3040.
[48] S. D. Dimitrov, S. Wheeler, D. Niedzialek, B. C. Schroeder, H. Utzat, J. M. Frost, J. Z. Yao, A. Gillett, P. S. Tuladhar, I. McCulloch, J. Nelson, J. R. Durrant, *Nat. Commun.* **2015**, *6*, 6501.
[49] R. Shivanna, S. Shoaee, S. Dimitrov, S. K. Kandappa, S. Rajaram, J. R. Durrant, K. S. Narayan, *Energy Environ Sci.* **2014**, *7*, 435.
[50] K. Kawashima, Y. Tamai, H. Ohkita, I. Osaka, K. Takimiya, *Nat. Commun.* **2015**, *6*, 10085.
[51] W. Zhao, D. Qian, S. Zhang, S. Li, O. Inganas, F. Gao, J. Hou, *Adv. Mater.* **2016**, *28*, 4734.
[52] K. R. Graham, C. Cabanetos, J. P. Jahnke, M. N. Idso, A. El Labban, G. O. Ngongang Ndjawa, T. Heumueller, K. Vandewal, A. Salleo, B. F. Chmelka, A. Amassian, P. M. Beaujuge, M. D. McGehee, *J. Am. Chem. Soc.* **2014**, *136*, 9608.
[53] N. A. Ran, J. A. Love, C. J. Takacs, A. Sadhanala, J. K. Beavers, S. D. Collins, Y. Huang, M. Wang, R. H. Friend, G. C. Bazan, T. Q. Nguyen, *Adv. Mater.* **2016**, *28*, 1482.
[54] K. Vandewal, K. Tvingstedt, A. Gadisa, O. Inganäs, J. V. Manca, *Phys. Rev. B* **2010**, *81*, 125204.
[55] D. Veldman, S. C. J. Meskers, R. A. J. Janssen, *Adv. Funct. Mater.* **2009**, *19*, 1939.

